ISSN 1070-3284, Russian Journal of Coordination Chemistry, 2022, Vol. 48, No. 10, pp. 659–666. © Pleiades Publishing, Ltd., 2022.

Syntheses, Crystal Structures, and Magnetic Properties of Two Cobalt(II) Coordination Complexes with 4'-Substituted 3,2':6',3''-Terpyridine Ligands

Y. J. Dong[a, b], W. W. Fu[b, *], S. Y. Gui[b], X. Liu[a], L. L. Zi[b], and L. S. Wang[a, **]

[a] *Hubei Provincial Key Laboratory of Green Materials for Light Industry, Collaborative Innovation Center of Green Light-Weight Materials and Processing, School of Material and Chemical Engineering, Hubei University of Technology, Wuhan, 430068 P.R. China*

[b] *Key Laboratory of Functional Metal-Organic Compounds of Hunan Province, Key Laboratory of Functional Organometallic Materials, University of Hunan Province, Hunan Provincial Engineering Research Center for Monitoring and Treatment of Heavy Metals Pollution in the Upper Reaches of Xiangjiang River, College of Chemistry and Materials Science, Hengyang Normal University, Hengyang, 421008 P.R. China*

**e-mail: w.w.fu@hynu.edu.cn*

***e-mail: wangls@mail.hbut.edu.cn*

Received December 1, 2021; revised March 6, 2022; accepted March 15, 2022

Abstract—Two new cobalt(II) coordination complexes $[Co(Phtpy)(HBTC)_{0.5}]_n \cdot nH_2O$ (**I**) and $[Co(Meophtpy)(HBTC)_{0.5}]_n \cdot nH_2O$ (**II**) (Phtpy = 4'-(4-phenyl)-3,2':6',3''-terpyridine, Meophtpy = 4'-(4-methoxyphenyl)-3,2':6',3''-terpyridine, H_3BTC = trimesic acid) were synthesized under solvothermal conditions. The structures of complexes **I**, **II** have been characterized by elemental analysis, FT-IR, TG analysis, PXRD and single crystal X-ray diffraction techniques (CCDC nos. 2123289 (**I**) and 2123290 (**II**)). For complex **I**, a two-dimensional (2D) layered structure is formed parallel to the *bc* plane and the adjacent layers are connected by Phtpy ligand along *a* direction to form a three-dimensional (3D) structure. It is represented as 2-nodal (3, 5)-connected $\{4.6.8\}\{4.6^6.8^3\}$ by Schläfli symbol. For complex **II**, one-dimensional (1D) ladder chains along two almost perpendicular directions are formed and these chains are connected by Meophtpy ligands to form a 3D structure. It is represented as 2-nodal (3, 5)-connected $\{4^2.6^5.8^3\}\{4^2.6\}$ by Schläfli symbol. In both complexes, dominant antiferromagnetic interactions between Co(II) ions were observed.

Keywords: metal-organic frameworks, terpyridine, crystal structure, trimesic acid, magnetic property

DOI: 10.1134/S1070328422100013

INTRODUCTION

In the past decades, reasonable design and construction of MOFs (metal-organic frameworks) have become one of the most attractive research topics not only for fascinating structures and topologies of MOFs [1–5], but also for their potential applications in magnetism [6], catalysis [7], luminescence [8], adsorption [9], and so on. Much attention has been focused on the purposeful design and controllable synthesis of MOFs employing self-assembly processes with polycarboxylate and N-heterocyclic ligands [10–12].

As aromatic polypyridine ligands, 4'-substituted-2,2':6',2''-terpyridine (2262-tpy) have been widely accepted in constructing MOFs with different polycarboxylates and transition metal ions. However, the cohesive terpyridyl moiety in 2262-tpy often acts as chelating group as all three N atoms on pyridyl groups coordinated to the same transition metal atoms, which limited the structural diversity and application of terpyridine complexes [13–15]. In contrast, the coordination mode of 4'-substituted-3,2':6',3''-terpyridine (3263-tpy) is significantly different from its 2262-tpy isomer because it contains two side exo-pyridyl groups and the N atoms on these exo-pyridyl groups are usually coordinated to different transition metal ions, which expended the structural diversity and application of terpyridine complexes [16–18].

In order to investigate the influence of different substitutes on the crystal structures and properties of 3263-tpy based MOFs, a series of mixed-ligand experiments with 4'-(4-phenyl)-3,2':6',3''-terpyridine [19] and 4'-(4-methoxyphenyl)-3,2':6',3''-terpyridine [20, 21] as N-donor bridging ligands and terephthalic acid, isophthalic acid or trimesic acid as O-donor polycarboxylate ligands for their abundant coordination modes [22] under employment of different transitional metal ions like Mn(II), Co(II), Ni(II), and Cu(II), as well as the careful selection of solvents,

temperatures and different ratios of reagent, have been performed in our laboratory as an continue of our previous work [15].

Fortunately, we obtained two Co(II) complexes $[Co(Phtpy)(HBTC)_{0.5}]_n \cdot nH_2O$ (**I**) and $[Co(Meophtpy)(HBTC)_{0.5}]_n \cdot nH_2O$ (**II**). Complex **I** represents a common example of 2D → 3D motif with Phtpy as linkers [23], as well as complex **II** represents a more common example of 1D → 3D with Meophtpy as linkers [24]. Just as MOFs containing transitional metal ions with unpaired electrons have potential application in the field of molecular magnetism and materials chemistry [25], especially for Co(II) complexes [26], the magnetic properties of complexes **I** and **II** have been investigated.

EXPERIMENTAL

Materials and methods. The ligands 4'-(4-Phenyl)-3,2':6',3''-terpyridine (Phtpy) and 4'-(4-methoxyphenyl)-3,2':6',3''-terpyridine (Meophtpy) were prepared according to literature methods with 3-acetylpyridine instead of 2-acetylpyridine [27]. All the other reagents and solvents were commercially available and used as received. Fourier-transform infrared spectra (FT-IR) were recorded on a Shimadzu Prestige-21 FT-IR spectrometer using dry KBr pellets from 4000–400 cm^{-1}. Elemental analyses were carried out on EA1110 CHNS-0 CE elemental analyzer. Thermogravimetric analyses (TGA) were carried out on a NetzschSTA499C integration thermal analyzer under a nitrogen atmosphere from room temperature to 700°C at a heating rate of 10°C/min. Magnetic susceptibility (χ) was measured using a Quantum Design PPMS-9 magnetometer in 1000 Oe field over the temperature range of 1.8–300 K.

Synthesis of $[Co(Phtpy)(HBTC)_{0.5}]_n \cdot nH_2O$ (I). A mixture of $Co(NO_3)_2 \cdot 6H_2O$ (0.029 g, 0.1 mmol), trimesic acid (0.021 g, 0.1 mmol), Phtpy (0.031 g, 0.1 mmol), CH_3CN (8 mL), and H_2O (2 mL) was sealed in a 15 mL Teflon-lined stainless steel vessels under autogenous pressure. Subsequently, red block crystals of complex **I** were grown from the solution after one week (the yield was 58% based on Co).

IR (KBr; ν, cm^{-1}): 1732 s, 1635 s, 1541 m, 1396 s, 1309 s, 1193 m, 1032 w, 812 m, 721 m, 690 m, 544 w.

For $C_{30}H_{21}N_3O_7Co$			
Anal. calcd., %	C, 60.62	H, 3.56	N, 7.07
Found, %	C, 60.53	H, 3.59	N, 7.21

Synthesis of $[Co(Meophtpy)(HBTC)_{0.5}]_n \cdot nH_2O$ (II). A mixture of $Co(NO_3)_2 \cdot 6H_2O$ (0.029 g, 0.1 mmol), trimesic acid (0.021 g, 0.1 mmol), Meophtpy (0.034 g, 0.1 mmol), CH_3CN (8 mL), and H_2O (2 mL) was sealed in a 15 mL Teflon-lined stainless steel vessels under autogenous pressure. Subsequently, red block crystals of complex **II** were grown from the solution after one week (the yield was 56.9% based on Co).

IR (KBr; ν, cm^{-1}): 1734 m, 1618 s, 1520 m, 1375 s, 1273 m, 1188 m, 1036 w, 816 m, 724 m, 573 w, 418 w.

For $C_{31}H_{23}N_3O_8Co$			
Anal. calcd., %	C, 59.62	H, 3.71	N, 6.73
Found, %	C, 59.28	H, 3.80	N, 6.68

X-ray structure determination. X-ray diffraction data for complexes **I** and **II** were collected on a Bruker SMART APEX-II CCD diffractometer equipped with a graphite crystal and incident beam monochromator using MoK_α radiation (λ = 0.71073 Å) by using the φ–ω scan technique at room temperature. All data are corrected by Lp factor and experience absorption. The crystal structures were solved and refined by the SHELXL-2014 procedure [28] with the graphical interface Olex2 [29]. The isotropic and anisotropic temperature factors for hydrogen atoms and non-hydrogen atoms are used for the whole matrix least square method correction. Crystal data, data collection parameters and analysis statistics are listed in Table 1. Selected bond lengths and angles are given in Table 2.

The full tables of interatomic distances and bond angles, atomic coordinates, and atomic displacement parameters were deposited with the Cambridge Crystallographic Data Centre (CCDC nos. 2123289 (**I**) and 2123290 (**II**); deposit@ccdc. cam.ac.uk or https://www.ccdc.cam.ac.uk/structures) and also can be requested from the authors.

RESULTS AND DISCUSSION

As depicted in Fig. 1a, the asymmetric unit of complex **I** contains one Co(II) ion, one Phtpy ligand, one $HBTC^{2-}$ anion and one lattice H_2O molecule. The coordination environment around Co(1) is described as a distorted octahedron. The Co(II) ions are coordinated by four carboxylate oxygen atoms from three different $HBTC^{2-}$ anions and two exo-pyridyl nitrogen atoms from two distinct Phtpy ligands. The bond lengths of Co–O bonds are 1.995(2)–2.252(3) Å, and the bond lengths of Co–N bonds are 2.154(3)–2.162(3) Å, respectively, all falling in the normal range [30]. The $HBTC^{2-}$ anion in **I** is partially deprotonated and acts as one μ_3-η^1:η^1:η^1:η^0 coordination mode [31] to form a two-dimensional (2D) layer structure along the *bc* plane (Fig. 1b). The Phtpy ligand appears as a binary bridged ligand, which coordinates with Co(II) ions along *a* axis to form a three-dimensional (3D) structure (Fig. 1c). The closest distance between adjacent two-dimensional layers of Co–Co is 13.387 Å. From topological viewpoint, Co(II) ions are coordinated by three $HBTC^{2-}$ anions and two Phtpy ligand,

Table 1. Crystallographic data and structure refinement information for complexes **I** and **II**

Parameter	Value	
	I	**II**
Empirical formula	$C_{30}H_{21}N_3O_7Co$	$C_{31}H_{23}N_3O_8Co$
Formula weight	594.43	624.45
Crystal system	Monoclinic	Monoclinic
Space group	*C*2/*c*	*C*2/*c*
a, Å	24.5487(13)	15.747(4)
b, Å	12.7790(7)	12.932(3)
c, Å	17.1728(9)	26.455(3)
β, deg	102.5850(10)	93.384(4)
V, Å^3	5257.8(5)	5378.3(18)
Z	8	8
ρ, g/cm^3	1.502	1.542
F(000)	2440	2568
Crystal size, mm	0.22 × 0.17 × 0.15	0.19 × 0.15 × 0.13
Goodness-of-fit on F^2	1.030	1.027
Reflections collected/unique	13342/4628	13056/4713
R_1, wR_2 ($I > 2\sigma(I)$)[a]	$R_1 = 0.0361$, $wR_2 = 0.0803$	$R_1 = 0.0485$, $wR_2 = 0.1102$
R_1, wR_2 (all data)[b]	$R_1 = 0.0542$, $wR_2 = 0.0867$	$R_1 = 0.0913$, $wR_2 = 0.1225$
Residual electron density (min/max), e/Å^3	−0.256, 0.250	−0.411, 0.441

[a] $R_1 = \Sigma\|F_o|-|F_c\|/\Sigma|F_o|$, [b] $wR_2 = \{\Sigma[w(F_o^2 - F_c^2)^2]/\Sigma[w(F_o^2)^2]\}^{1/2}$.

respectively, which are considered as 5-connected nodes. The $HBTC^{2-}$ anion links three Co(II) ions, which is considered as a 3-connected node. The Phtpy ligand connects two metal Co(II) ions as a linker. The final structure is simplified as 2-nodal (3, 5)-connected {4.6.8}{$4.6^6.8^3$} framework (Fig. 1d).

As depicted in Fig. 2a, the asymmetric unit of complex **II** contains one Co(II) ion, one Meophtpy ligand, one $HBTC^{2-}$ anion and one lattice H_2O molecule. The coordination environment around Co(1) is described as a distorted octohedron, too. The Co(II) ions are coordinated by four carboxylate oxygen atoms from three different $HBTC^{2-}$ anions and two exo-pyridyl nitrogen atoms from two distinct Meophtpy ligands. The bond length of Co–O bonds are 2.039(2)–2.223(3) Å, and the bond length of Co–N bonds are 2.133(3)–2.137(3) Å, respectively, all falling in the normal range [30]. The $HBTC^{2-}$ anion in **II** is partially deprotonated and acts also as one μ_3-η^1:η^1:η^1:η^0 coordination mode [31] to form one-dimensional (1D) ladder chains (Fig. 2b) along two almost perpendicular directions and the Meophtpy ligands link the 1D ladder chains with different propagating direction to form a 3D framework (Fig. 2c). From topological viewpoint, Co(II) ions are coordinated by three $HBTC^{2-}$ anions and two Meophtpy ligands, respectively, which are considered as 5-connected nodes. The $HBTC^{2-}$ anion links three Co(II) ions, which is considered as a 3-connected node. The Meophtpy ligand connects two metal Co(II) ions as a linker. The final structure is simplified as 2-nodal (3, 5)-connected {$4^2.6^5.8^3$}{$4^2.6$} framework (Fig. 2d). These 1D ladder chains are arranged on parallel levels in two propagating directions (Fig. 2e), resulting in an AABB sequence in 2D stacking.

Table 2. Selected bond lengths (Å) and bond angles (deg) of complexes **I** and **II**

Bond	*d*, Å	Bond	*d*, Å
		I	
Co(1)–O(1)	1.9947(15)	Co(1)–O(3)$^{\#2}$	2.1609(16)
Co(1)–O(2)$^{\#1}$	2.0090(15)	Co(1)–N(3)$^{\#3}$	2.162(2)
Co(1)–N(1)	2.154(2)	Co(1)–O(4)$^{\#2}$	2.2525(16)
		II	
Co(1)–O(1)	2.039(2)	Co(1)–N(3)$^{\#3}$	2.137(3)
Co(1)–O(2)$^{\#1}$	2.057(2)	Co(1)–O(3)$^{\#2}$	2.206(2)
Co(1)–N(1)	2.133(3)	Co(1)–O(4)$^{\#2}$	2.223(2)
Angle	ω, deg	Angle	ω, deg
		I	
O(1)Co(1)O(2)$^{\#1}$	122.13(7)	N(1)Co(1)N(3)$^{\#3}$	174.46(7)
O(1)Co(1)N(1)	89.04(7)	O(3)$^{\#2}$Co(1)N(3)$^{\#3}$	85.30(7)
O(2)$^{\#1}$Co(1)N(1)	93.75(7)	O(1)Co(1)O(4)$^{\#2}$	91.68(6)
O(1)Co(1)O(3)$^{\#2}$	149.37(6)	O(2)$^{\#1}$Co(1)O(4)$^{\#2}$	146.18(6)
O(2)$^{\#1}$Co(1)O(3)$^{\#2}$	87.33(6)	N(1)Co(1)O(4)$^{\#2}$	86.99(7)
N(1)Co(1)O(3)$^{\#2}$	97.81(7)	O(3)$^{\#2}$Co(1)O(4)$^{\#2}$	59.16(6)
O(1)Co(1)N(3)$^{\#3}$	85.99(7)	N(3)$^{\#3}$Co(1)O(4)$^{\#2}$	90.71(7)
O(2)$^{\#1}$Co(1)N(3)$^{\#3}$	90.96(7)		
		II	
O(1)Co(1)O(2)$^{\#1}$	119.22(10)	N(1)Co(1)N(3)$^{\#3}$	89.82(10)
O(1)Co(1)N(1)	91.55(10)	N(3)$^{\#3}$Co(1)O(3)$^{\#2}$	94.13(10)
O(2)$^{\#1}$Co(1)N(1)	88.69(10)	O(1)Co(1)O(4)$^{\#2}$	147.09(9)
O(1)Co(1)N(3)$^{\#2}$	87.56(10)	O(2)$^{\#1}$Co(1)O(4)$^{\#2}$	93.59(9)
O(2)$^{\#1}$Co(1)N(3)$^{\#3}$	88.27(10)	N(1)Co(1)O(4)$^{\#2}$	91.72(10)
N(1)Co(1)N(3)$^{\#3}$	175.92(11)	N(3)$^{\#3}$Co(1)O(4)$^{\#2}$	91.19(10)
O(1)Co(1)O(3)$^{\#2}$	88.38(9)	O(3)$^{\#2}$Co(1)O(4)$^{\#2}$	58.89(9)
O(2)$^{\#1}$Co(1)O(3)$^{\#2}$	152.39(9)		

Symmetry codes: $^{\#1}$ $-x+1/2, -y+1/2, -z$; $^{\#2}$ $-x+1/2, y-1/2, -z-1/2$; $^{\#3}$ $x-1/2, -y+1/2, z-1/2$ (**I**). $^{\#1}$ $-x, -y, -z$; $^{\#2}$ $-x+1/2, -y+1/2, -z$; $^{\#3}$ $x, -y, z-1/2$ (**II**).

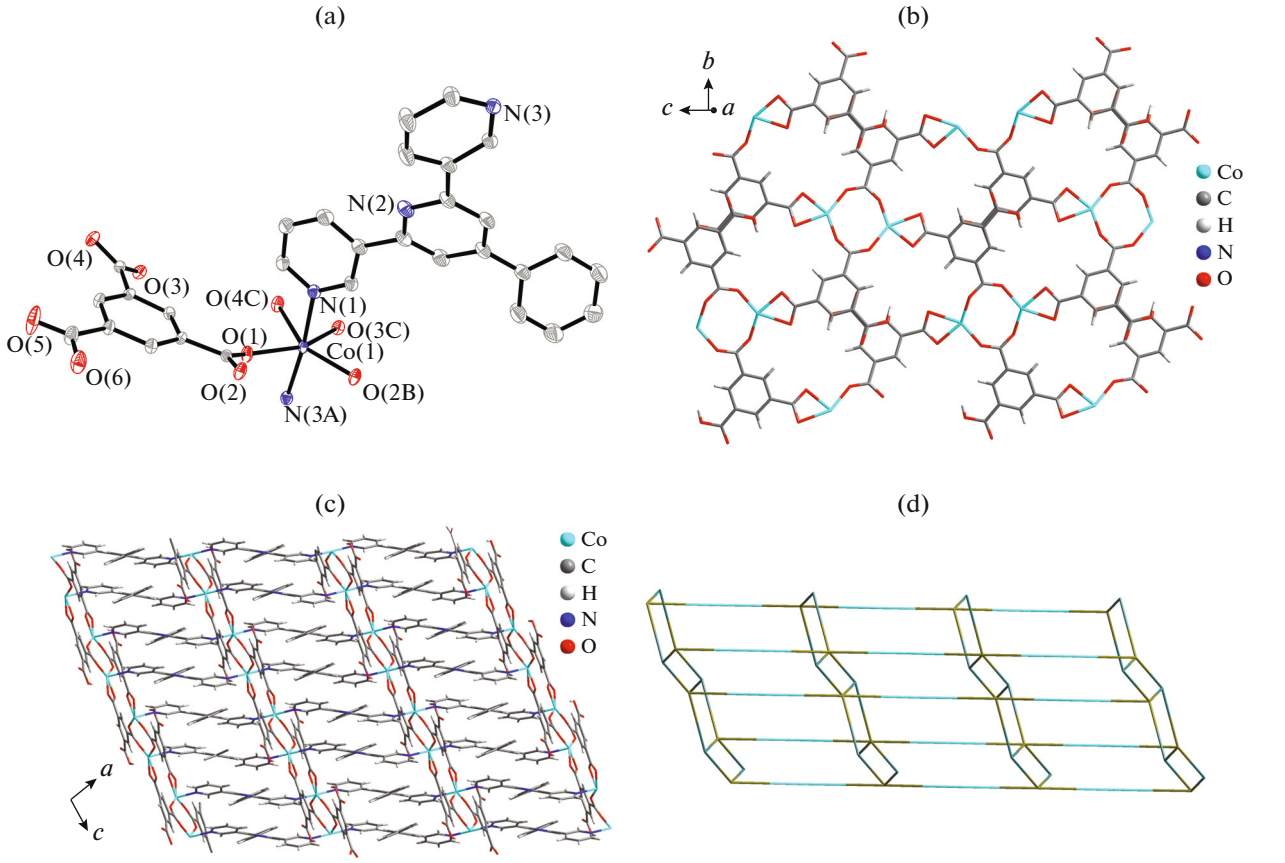

Fig. 1. Coordination environment of Co(II) in **I** showing 30% probability displacement ellipsoids (H atoms are omitted for clarity). Symmetry codes: (A) $-x + 1/2, -y + 1/2, -z$; (B) $-x + 1/2, y - 1/2, -z - 1/2$; (C) $x - 1/2, -y + 1/2, z - 1/2$ (a); the 2D layer structure of **I** (b); the 3D supramolecular network of **I** (c); the simplified 3D network of **I** with (3, 5) topology (d).

In order to check the phase purity of complexes **I** and **II**, PXRD patterns were recorded at room temperature (Fig. 3). The experimental and simulated PXRD patterns agree well with each other, confirming the good phase purity. The slight difference in intensity may arise from the preferred orientation of crystalline powder samples.

In order to study the thermal stability of complexes **I** and **II**, TGA was carried out, and the results are shown in Fig. 4. In complex **I**, a fast mass loss can be observed from room temperature to 188°C, and the weight loss is attributed to removal of water molecules (calcd. 3.03%, found 2.80%). Then, there is a plateau in the mass loss until the second step mass loss starts, which was observed from 379 to 633°C, and it should be ascribed as the decomposition of organic ligand just as the final residue is CoO (calcd. 13.00%, found 14.10%) [32]. In complex **II**, it also contains two weight loss steps, in which the first observed from room temperature to 186°C corresponding to the loss of the lattice water molecules (calcd. 2.88%, found 2.63%). Then, there is also a plateau until the second weight loss step began at 380°C corresponding to the decomposition of organic ligands. The remaining weight of the final residue of **II** is also presumed to be CoO (calcd. 12.36%, found 13.94%).

The magnetic behaviors of complexes **I** and **II** have been measured in a temperature range of 1.8–300 K under an applied magnetic field of 1000 Oe. Their χ_M^{-1} and $\chi_M T$ versus T plots are shown in Fig. 5 (χ_M is the magnetic susceptibility per formula unit). The $\chi_M T$ values at 300 K for **I** and **II** are 3.60 and 3.43 $cm^3\ mol^{-1}\ K$, respectively, much higher than the spin-only value 1.875 $cm^3\ mol^{-1}\ K$ expected for one uncoupled high-spin Co(II) ion ($S = 3/2$, $g = 2$), which is due to the contributions from an orbital angular momentum of the Co(II) ion at high temperatures [32–36]. When the temperature is decreased from 300 to 1.8 K, the $\chi_M T$ values decline slowly up to around 10 K, below which they decrease in a relatively rapid manner and reach local minimums of 0.41 and 1.11 $cm^3\ mol^{-1}\ K$ at 1.8 K, respectively. Above 100 K, the susceptibilities of **I** and **II** obey the Curie–Weiss law, $\chi_M = C/(T - \theta)$, giving the Weiss constants $\theta = -40.18$ and -36.41 K, and the Curie constant $C = 4.04$ and 3.82 $cm^3\ mol^{-1}\ K$, respectively. Both the trend of $\chi_M T$ versus T and the negative values of θ indicate the antiferromagnetic

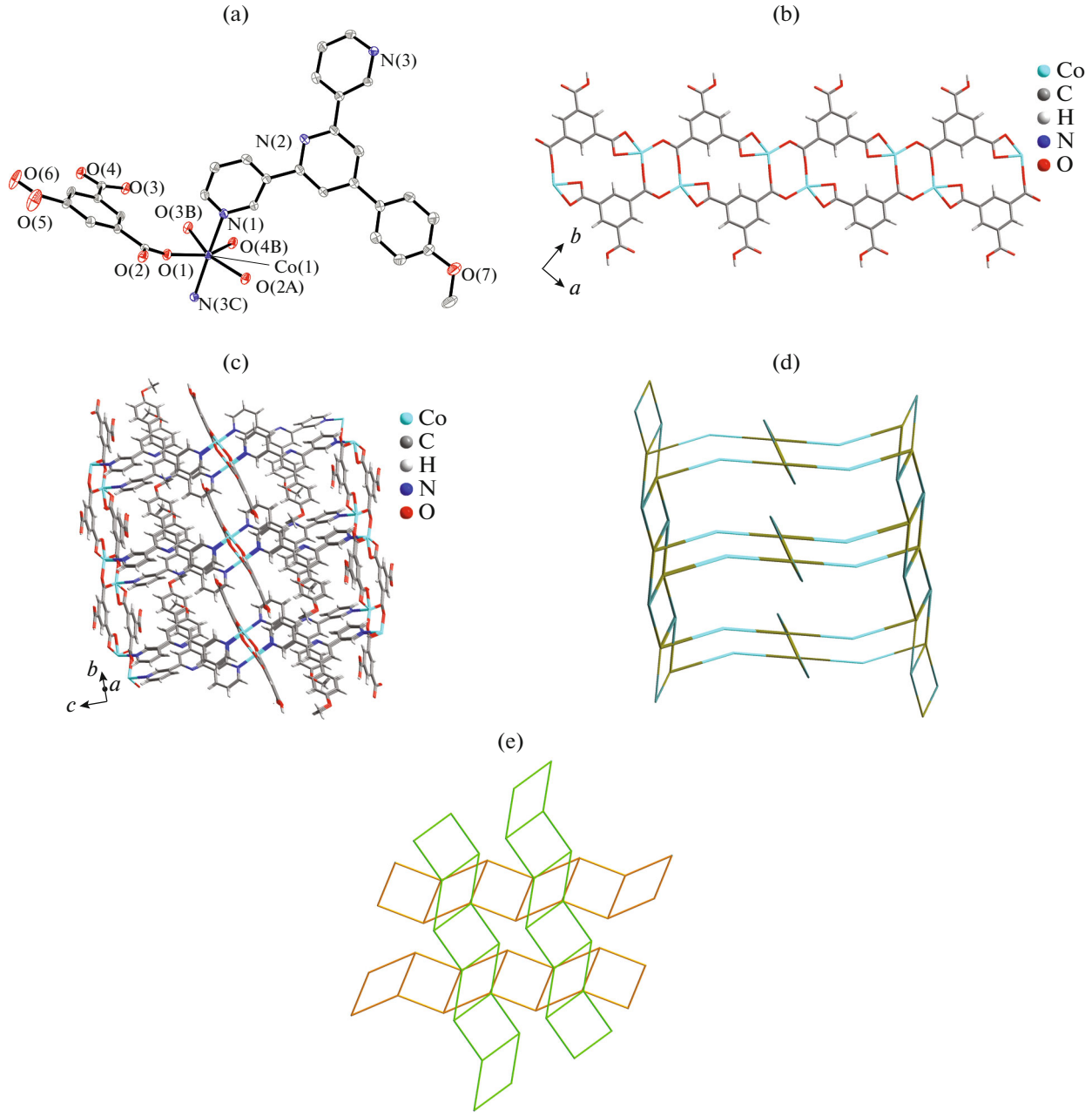

Fig. 2. Coordination environment of Co(II) in **II** showing 30% probability displacement ellipsoids (H atoms are omitted for clarity). Symmetry codes: (A) $-x, -y, -z$; (B) $-x + 1/2, -y + 1/2, -z$; (C) $x, -y, z - 1/2$ (a); the 1D ladder chain in **II** (b); the 3D supramolecular network of **II** (c); the simplified 3D network of **II** with (3, 5) topology with 1D ladder chains (the green and brown color showing 1D ladder chains along different directions) (d); packing diagram of the simplified 1D ladder chains in **II** along different directions (e).

interactions within the $Co_2(CO_2)_2$ dimer [33, 34, 36–38]. In addition, both the moderate negative θ values [33] and the reducing of the $\chi_M T$ magnitude from 10 to 1.8 K until it is less than spin-only values [35–38] indicate the predominance of antiferromagnetic interactions between Co^{2+} ions in the obtained complexes.

The distances between the neighboring Co(II) ions of **I** linked by different carboxylate groups of $HBTC^{2-}$ and Phtpy ligands are 7.923 and 13.387 Å and the distances between the neighboring Co(II) ions of **II** linked by $HBTC^{2-}$ and Meophtpy ligands are 7.575 and 13.228 Å, respectively, while that linked by the same carboxylate groups of $HBTC^{2-}$ are 4.067 Å for **I** and 4.125 Å for **II**. It is obvious that the significant Co(II)–Co(II) magnetic exchange interaction is transmitted through the bridging carboxylate groups of $HBTC^{2-}$ in a syn-syn mode [34, 38]. There are also

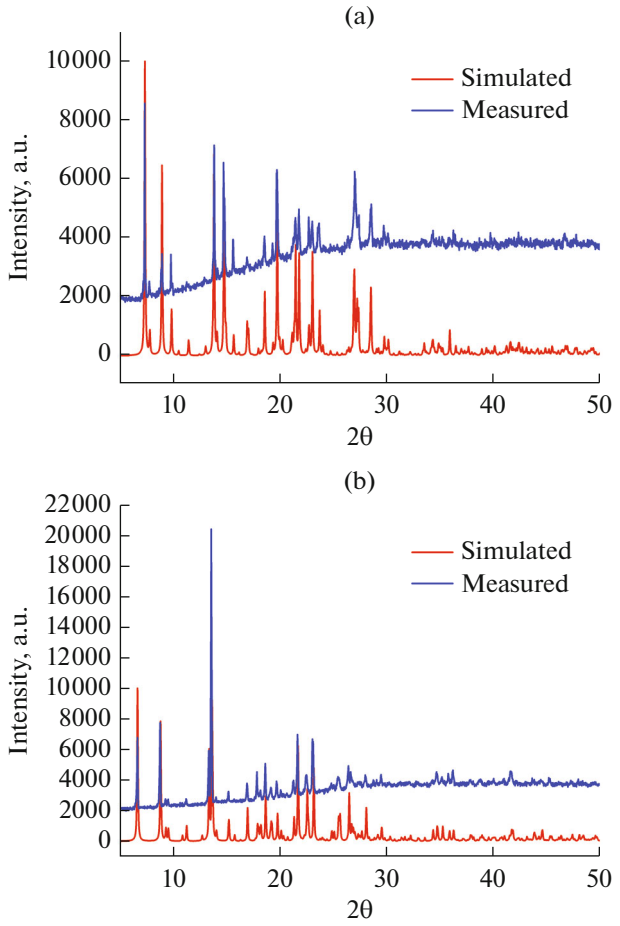

Fig. 3. PXRD patterns of **I** (a) and **II** (b).

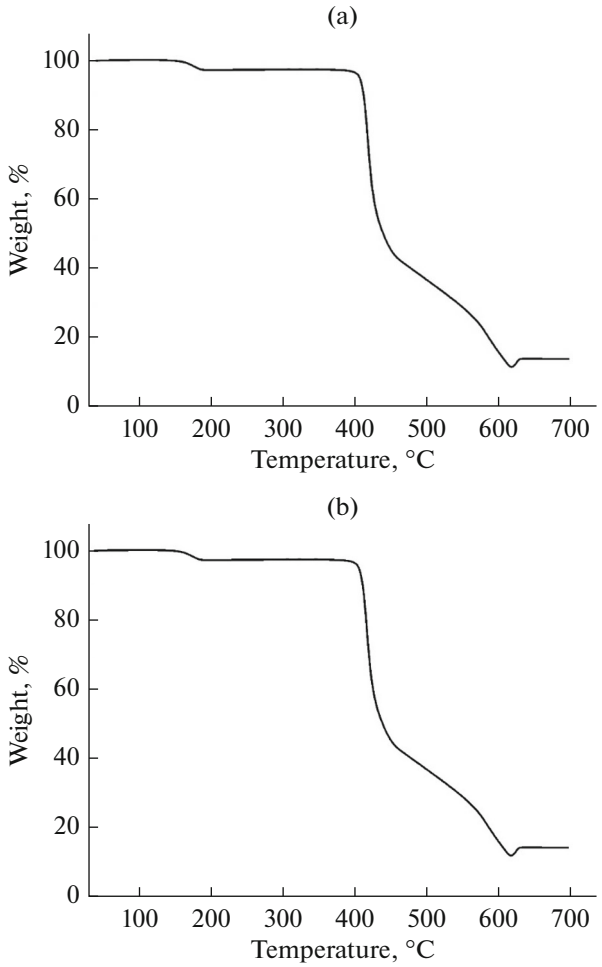

Fig. 4. TGA curves of **I** (a) and **II** (b).

some reports about the structures [39] and magnetic properties of 3263-tpy Co(II) coordination complexes [12, 40, 41], all with a distorted octahedron enviroment for Co(II) ions and antiferromagnetic interactions between Co(II) ions. However, no $Co_2(CO_2)_2$ dimer structures composed of 3263-tpy have been found. Just as the properties of coordination complexes are determined by their structures, the small differences of $\chi_M T$ values for **I** and **II** are correlated with the slight structure differences, e.g. the nearest Co–Co distances.

In summary, self-assembly of Co(II) salts with 4'-substituted-3,2':6',3''-terpyridine and trimesic acid ligands produced two MOFs. Although both complexes are 3D and simplified as 2-nodal (3, 5)-connected networks, their structures are different. Complex **I** is constructed with 2D layers by Phtpy as linkers [19], while complex **II** is constructed with 1D ladder chains by Meophtpy as linkers, showing the important influence of substitutes like Methoxy group on the structures of complexes. The variable-temperature magnetic susceptibility data reveal that both complexes exhibit dominant antiferromagnetic interactions.

FUNDING

This work was supported by Open Research Foundation of Hubei Provincial Key Laboratory of Green Materials for Light Industry and Collaborative Innovation Center of Green Light-Weight Materials and Processing of Hubei University of Technology (no. 201611B16), the Scientific Research Fund of Hunan Provincial Education Department (no. 20K016), the Foundation of Key Laboratory of Functional Metal-Organic Compounds of Hunan Province (no. MO19K02), Youth Chutian Scholar Fund of Hubei Province (no. 4032401), State Key Laboratory of Structural Chemistry (no. 20180023), Hubei Provincial Key Laboratory of Green Materials for Light Industry (no. 201907A09).

CONFLICT OF INTEREST

The authors declare that they have no conflicts of interest.

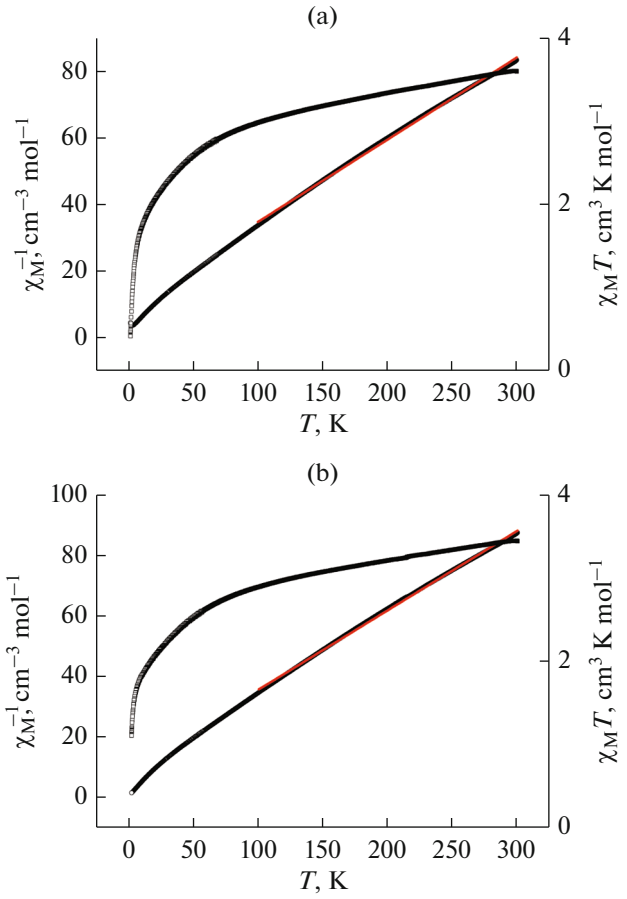

Fig. 5. Temperature dependence of $\chi_M T$ and χ_M^{-1} for **I** (a) and **II** (b). The red solid line shows the Curie–Weiss fit.

REFERENCES

1. Schoedel, A., Li, M., Li, D., et al., *Chem. Rev.*, 2016, vol. 116, p. 12466.
2. Saad, A., Biswas, S., and Gkaniatsou, E., *Chem. Mater.*, 2021, vol. 33, p. 5825.
3. Ohrstrom, L., *Crystals*, 2015, vol. 5, p. 154.
4. Aljammal, N., Jabbour, C., Chaemchuen, S., et al., *Catalysts*, 2019, vol. 9, p. 31.
5. Zhao, D., Timmons, D.J., Yuan, D.Q., and Zhou, H.C., *Accounts. Chem. Res.*, 2011, vol. 44, p. 123.
6. Espallargas, G.M. and Coronado, E., *Chem. Soc. Rev.*, 2018, vol. 47, p. 533.
7. Huang, Y.B., Liang, J., Wang, X.S., and Cao, R., *Chem. Soc. Rev.*, 2017, vol. 46, p. 126.
8. Lustig, W.P., Mukherjee, S., Rudd, N.D., et al., *Chem. Soc. Rev.*, 2017, vol. 46, p. 3242.
9. Fan, W.D., Wang, X., Xu, B., et al., *J. Mater. Chem. A*, 2018, vol. 6, p. 24486.
10. Sun, D., Xu, M.Z., Liu, S.S., et al., *Dalton Trans.*, 2013, vol. 42, p. 12324.
11. Bai, N.N., Hou, L., Gao, R.C., et al., *CrystEngComm*, 2017, vol. 19, p. 4789.
12. Zheng, L.N., Cheng, Y., Hu, et al., *J. Solid. State. Chem.*, 2019, vol. 272, p. 210.
13. Ma, Z., Lu, W.B., Liang, B.H., and Pombeiro, A.J.L., *New J. Chem.*, 2013, vol. 37, p. 1529.
14. Lian, Z.X., Zhao, N., Liu, P., et al., *Z. Naturforsch., B: Chem. Sci.*, 2017, vol. 72, p. 125.
15. Fu, W.W., Ye, S.Q., Liu, Y., et al., *Transition Met. Chem.*, 2015, vol. 40, p. 227.
16. Wang, T.T., Zhang, J.L., Hu, H.M., et al., *Polyhedron*, 2018, vol. 151, p. 43.
17. Li, L., Zhang, Y.Z., Yang, C.X., et al., *Polyhedron*, 2016, vol. 105, p. 115.
18. Zhang, L., Li, C.J., He, J.E., et al., *J. Solid. State. Chem.*, 2016, vol. 233, p. 444.
19. Granifo, J., Vargas, M., Garland, M.T., et al., *Inorg. Chem. Commun.*, 2008, vol. 11, p. 1388.
20. Rocco, D., Prescimone, A., Klein, Y.M., et al., *Polymers*, 2019, vol. 11, p. 1224.
21. Rocco, D., Manfroni, G., Prescimone, A., et al., *Polymers*, 2020, vol. 12, p. 318.
22. Guo, X.G., Yang, W.B., Wu, X.Y., et al., *Dalton Trans.*, 2013, vol. 42, p. 15106.
23. Wu, H., Lu, X.L., Yang, C.L., et al., *CrystEngComm*, 2014, vol. 16, p. 992.
24. Zhou, X.H., Chen, Q.Q., Liu, B.L., et al., *Dalton Trans.*, 2017, vol. 46, p. 430.
25. Liu, J.L., Chen, Y.C., Guo, F.S., and Tong, M.L., *Coord. Chem. Rev.*, 2014, vol. 281, p. 26.
26. Kurmoo, M., *Chem. Soc. Rev.*, 2009, vol. 38, p. 1353.
27. Wang, J. and Hanan, G.S., *Synlett*, 2005, p. 1251.
28. Sheldrick, G., *Acta Crystallogr., Sect. C: Cryst. Struct. Chem.*, 2015, vol. 71, p. 3.
29. Dolomanov, O.V., Bourhis, L.J., Gildea, R.J., et al., *J. Appl. Crystallogr.*, 2009, vol. 42, p. 339.
30. Park, I.H., Ju, H., Herng, T.S., et al., *Cryst. Growth. Des.*, 2016, vol. 16, p. 7278.
31. Han, Z., Fu, Y.M., Zhang, Y.C., et al., *Dalton Trans.*, 2021, vol. 50, p. 3186.
32. Wang, X.L., Sui, F.F., Lin, H.Y., et al., *Cryst. Growth. Des.*, 2014, vol. 14, p. 3438.
33. Ma, L.F., Wang, L.Y., Wang, Y.Y., et al., *Inorg. Chem.*, 2009, vol. 48, p. 915.
34. Zhang, S.Y., Zhang, Z.J., Shi, W., et al., *Dalton Trans.*, 2011, vol. 40, p. 7993.
35. Dong, W.W., Li, D.S., Zhao, J., et al., *RSC Adv.*, 2012, vol. 2, p. 11219.
36. Lin, S.X., Liu, Y.Y., Wang, Z.X., et al., *Inorg. Chim. Acta*, 2019, vol. 497, p. 119083.
37. Huang, F.P., Tian, J.L., Gu, W., et al., *Cryst. Growth. Des.*, 2010, vol. 10, p. 1145.
38. Goswami, S., Leitus, G., Tripuramallu, B.K., and Goldberg, I., *Cryst. Growth. Des.*, 2017, vol. 17, p. 4393.
39. Yang, P., Wang, M.S., Shen, J.J., et al., *Dalton Trans.*, 2014, vol. 43, p. 1460.
40. Toledo, D., Peña, O., Roisnel, T., et al., Y., *J. Coord. Chem.*, 2018, vol. 71, p. 22.
41. Zhang, T.H., Bai, C., Hu, H.M., et al., *J. Solid. State. Chem.*, 2021, vol. 298, p. 122148.